Computational Engineering and Technology Innovations

www.ceti.reapress.com

Comput. Eng. Technol. Innov. Vol. 2, No. 3 (2025) 219–228.

Paper Type: Original Article

On Application of Partial Differential Equations to Model of Technological Process During in-Creasing of Integration Rate of Complementary Gate Overlap Field-Effect Heterotransistors in the Framework of a Double Tail Comparator

E. L. Pankratov*

[1] Nizhny Novgorod Article Agrotechnical University, 97 Gagarin Avenue, Nizhny Novgorod, 603950, Russia; elp2004@mail.ru.

Citation:

Received: 12 July 2024 *Revised: 02 August 2024* *Accepted: 18 March 2025*	Pankratov, E. L. (2025). On application of partial differential equations to model of technological process during in-creasing of integration rate of complementary gate overlap field-effect heterotransistors in the framework of a double tail comparator. *Computational engineering and technology innovations, 2*(3), 219-228.

Abstract

In this paper, we propose an approach for increasing the integration density of complementary gate overlap field-effect heterotransistors within the framework of a double-tail comparator. The pro-posed approach is based on the use of a heterostructure with a specially designed configuration. Several designated regions of the heterostructure are selectively doped using diffusion and/or ion implantation techniques. The subsequent annealing process, aimed at activating dopants and repair-ing radiation-induced defects, is subject to optimization.To predict and analyze the technological process, we develop a comprehensive mathematical model based on a system of partial differential equations. Furthermore, an analytical approach is employed to investigate the proposed model. This approach enables the consideration of both spatial and tem-poral variations of the model parameters, as well as the inherent nonlinearities of the underlying physical processes.

Keywords: Complementary gate overlaps field-effect heterotransistors, Double tail comparator, Opti-mization of manufacturing, Analytical approach for prognosis.

1 | Introduction

One of the most critical and actively researched challenges in solid-state electronics is the enhancement of the integration density of integrated circuit components, including p–n junctions and their functional

Corresponding Author: elp2004@mail.ru

https://doi.org/10.48314/ceti.v2i3.64 .

Licensee System Analytics. This article is an open access article distributed under the terms and conditions of the Creative Commons Attribution (CC BY) license (http://creativecommons.org/licenses/by/4.0).

assemblies [1–5]. The continuous demand for higher performance, lower power consumption, and reduced chip area has made dimensional scaling a key requirement in modern micro- and nanoelectronics technologies. As a result, increasing the integration density inevitably requires a substantial reduction in the physical dimensions of individual circuit elements [6–8].

To achieve this goal, several advanced technological approaches have been developed and extensively investigated. Among them, laser and microwave annealing techniques for introduced dopants have gained significant attention. These annealing methods are also widely employed for the elimination of radiation-induced defects generated during ion implantation processes. Compared with conventional thermal annealing, laser and microwave annealing provide improved control over thermal budgets and enable localized heating, which is particularly advantageous for nanoscale device fabrication [9–13].

The use of such annealing techniques allows an increase in the integration density of integrated circuit elements by intentionally introducing spatial inhomogeneities in technological parameters, primarily through the formation of nonuniform temperature distributions. Under these conditions, the characteristic dimensions of device elements can be effectively reduced, as dictated by the Arrhenius law governing thermally activated processes [1], [3], [14]. This approach makes it possible to tailor diffusion lengths and activation profiles, thereby enabling more precise control over junction depths and lateral dimensions.

Another widely used approach for fabricating integrated circuit elements with reduced dimensions involves the doping of heterostructures using diffusion or ion implantation techniques [1–3]. Heterostructures provide additional degrees of freedom for controlling carrier transport and junction properties due to their material composition and band structure engineering. However, the successful implementation of this approach requires careful optimization of dopant activation and the annealing of radiation-induced defects, as improper thermal treatment may degrade device performance or structural integrity [14].

In this paper, we consider a heterostructure consisting of a substrate and multiple epitaxial layers. Specific regions are formed within the epitaxial layers to define the functional sections of the device. These regions are subsequently doped using diffusion and/or ion implantation techniques. Such doping enables the fabrication of complementary gate overlap field-effect heterotransistors within the framework of a double-tail comparator, as illustrated in *Fig. 1*.

The proposed fabrication approach allows for a significant increase in the packing density of the comparator circuit elements by reducing the characteristic dimensions of individual device components. Following the doping process, the introduced dopants and/or radiation-induced defects must undergo annealing to achieve the required electrical activation and to restore the crystal lattice. Within the scope of this study, we analyze the dynamics of dopant redistribution and the evolution of radiation-induced defects during the annealing process. Particular attention is paid to the spatial and temporal behavior of these processes, as they critically influence the final device geometry and performance.

Based on this analysis, we propose an approach for reducing the dimensions of the device elements. However, the implementation of this approach necessitates a more complex technological process, which must be carefully optimized to balance fabrication complexity and device.

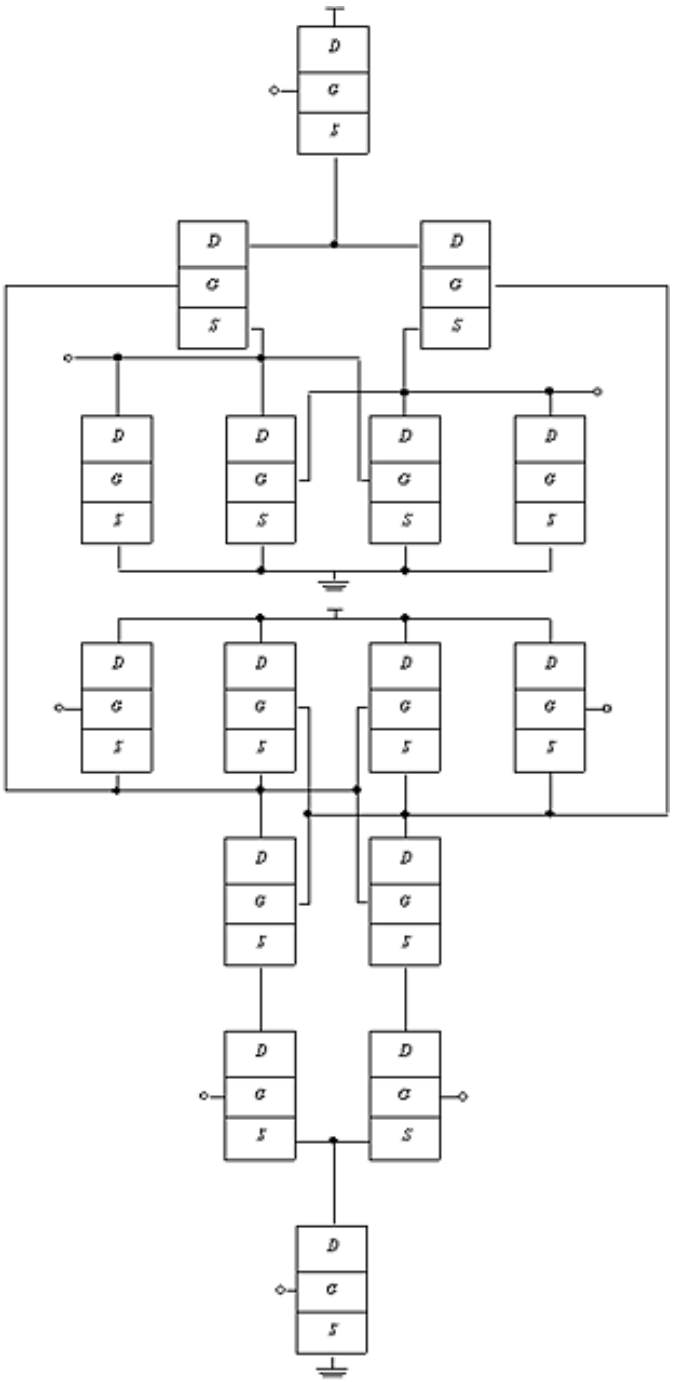


Fig. 1. The considered comparator [15].

2 | Method of Solution

In this section, we determine the spatial-temporal distributions of dopant atoms introduced by diffusion or ion implantation, as well as radiation-induced defects generated during the technological process. The evolution of the dopant concentration is governed by the second Fick's law [1], [3], [14].

$$\frac{\partial C(x,y,z,t)}{\partial t} = \nabla.(D_C \nabla C(x,y,z,t)), \quad (1)$$

where $C(x,y,z,t)$ is the dopant concentration and D_C is the dopant diffusion coefficient. The boundary and initial conditions correspond to zero-flux boundaries and a prescribed initial dopant distribution.

The dopant diffusion coefficient depends on the heterostructure material, annealing temperature, dopant concentration, and radiation defect density. Following Refs. [8], [14], [16–18], this dependence is approximated as

$$D_c = D_l(x, y, z, T)\left[1 + \gamma\frac{C}{P(x, y, z, T}\right]\left[1 + \xi\frac{V(x, y, z, t)}{V^*}\right], \quad (2)$$

where $D_L$accounts for spatial and temperature dependences in accordance with the Arrhenius law, Pis the dopant solubility limit, Vis the vacancy concentration, and $V^*$is its equilibrium value. In the case of diffusion-based doping, radiation defects are absent and the corresponding terms vanish.

For ion implantation, radiation-induced point defects such as vacancies Vand interstitials Iare generated. Their spatio-temporal evolution is described by a coupled system of diffusion–reaction equations [14], [16], which accounts for defect diffusion, recombination, and the formation of simple defect complexes. In compact form, this system can be written as

$$\frac{\partial\rho}{\partial t} = \nabla\cdot\left(D_\rho\nabla\rho\right) - k_{I,V}IV + G_\rho, \rho = I, V, \quad (3)$$

where D_ρ are the diffusion coefficients of point defects, $k_{I,V}$ is the recombination rate, and $G_\rho$represents generation terms associated with defect complexes.

The formation and evolution of divacancies and interstitials are described by similar diffusion equations with decay terms. Detailed formulations, boundary conditions, and reaction parameters are provided in the Appendix to avoid excessive mathematical complexity in the main text.

To obtain analytical solutions, we employ a perturbation-based approach recently developed in Ref. [14] Spatially and temperature-dependent diffusion coefficients and reaction parameters are expressed as small deviations from their average values, for example,

$$D_\rho(x, y, z, T) = D_{\rho0}\left[1 + \varepsilon_\rho g_\rho(x, y, z, T)\right], \quad (4)$$

with $0 \le \varepsilon_\rho < 1$. Dimensionless spatial variables are then introduced to simplify the governing equations.

The concentrations of dopants and radiation defects are sought in the form of power-series expansions with respect to the perturbation parameters. Substitution of these expansions into the governing equations yields a sequence of linear problems for the zero-order approximations and higher-order corrections. These problems are solved analytically using standard Fourier techniques [19], [20]. Explicit expressions for the solutions are presented in the Appendix.

All results are obtained within the second-order approximation, which provides sufficient accuracy for both qualitative analysis and quantitative predictions. The analytical results are verified by numerical simulations, demonstrating good agreement between the two approaches

3 | Discussion

In this section, we analyze the spatial-temporal distributions of dopant concentrations obtained from the proposed model. *Fig. 2* illustrates typical spatial profiles of dopant concentration in the vicinity of heterostructure interfaces. The presented distributions are calculated under the condition that the dopant diffusion coefficient within the doped region is higher than that in the adjacent layers.

Under these conditions, an increase in the compactness of field-effect transistors is observed, accompanied by an improvement in the homogeneity of the dopant concentration distribution. This behavior can be attributed to enhanced dopant redistribution within the active region, which promotes more uniform junction formation while limiting excessive diffusion into neighboring layers.

Conversely, altering the ratio between the diffusion coefficients of the doped region and the surrounding areas leads to the opposite effect, as shown in *Fig. 3*. In this case, reduced dopant confinement results in less

uniform concentration profiles and increased lateral spreading, which negatively affects device compactness and integration density

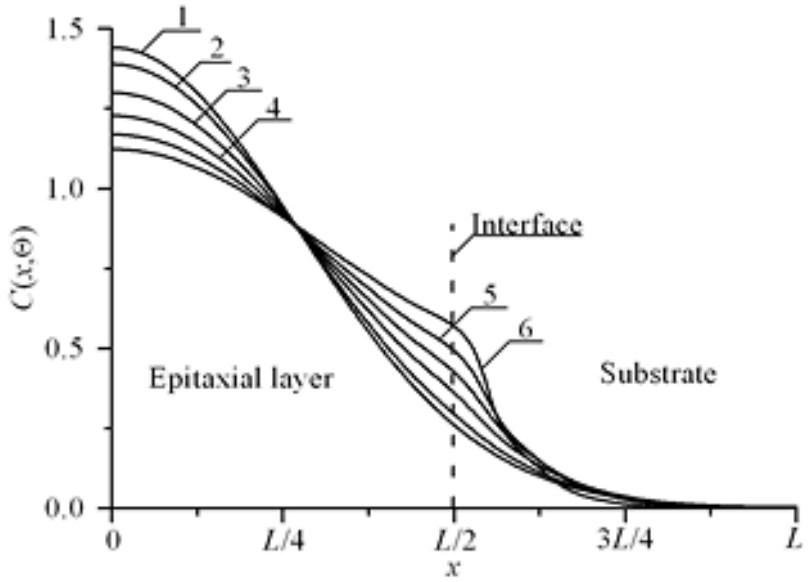


Fig. 2. Dopant concentration profiles in the heterostructure.

as a function of the coordinate perpendicular to the interface between the epitaxial layer and the substrate. The difference between the dopant diffusion coefficients in the heterostructure layers increases with the number of curves. The dopant diffusion coefficient in the epitaxial layer is higher than that in the substrate.

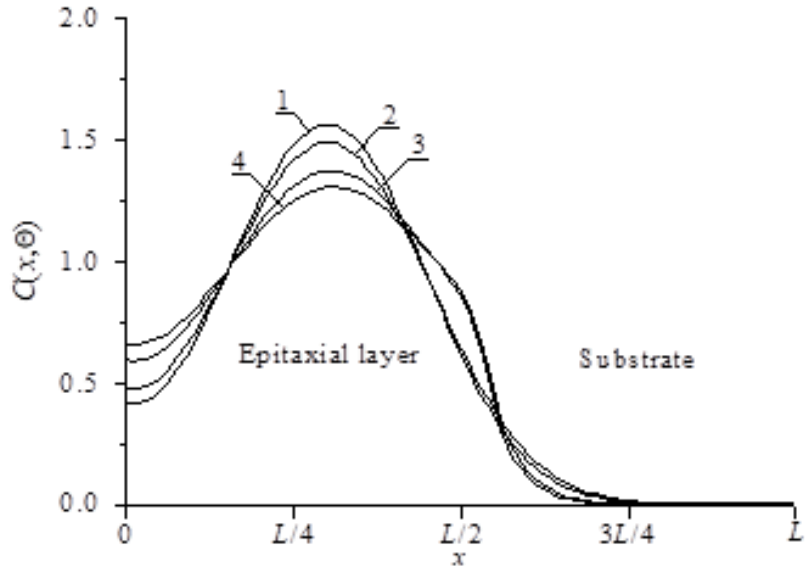


Fig. 3. Dependences of concentration of dopant, implanted in heterostructure.

Fig. 2. Dopant concentration profiles along the coordinate perpendicular to the interface between the epitaxial layer and the substrate. The difference between dopant diffusion coefficients in the heterostructure layers increases with the number of curves. The diffusion coefficient in the epitaxial layer is higher than in the substrate. Curve 1 represents a homogeneous sample with an annealing time of $\Theta = 0.0048(L_x^2 + L_y^2 + L_z^2)/D_0$, while Curve 2 corresponds to a homogeneous sample with $\Theta = 0.0057(L_x^2 + L_y^2 + L_z^2)/D_0$. Curves 3 and 4 correspond to the heterostructure shown in *Fig. 1*, with annealing times $\Theta = 0.0048(L_x^2 + L_y^2 + L_z^2)/D_0$and $\Theta = 0.0057(L_x^2 + L_y^2 + L_z^2)/D_0$, respectively.

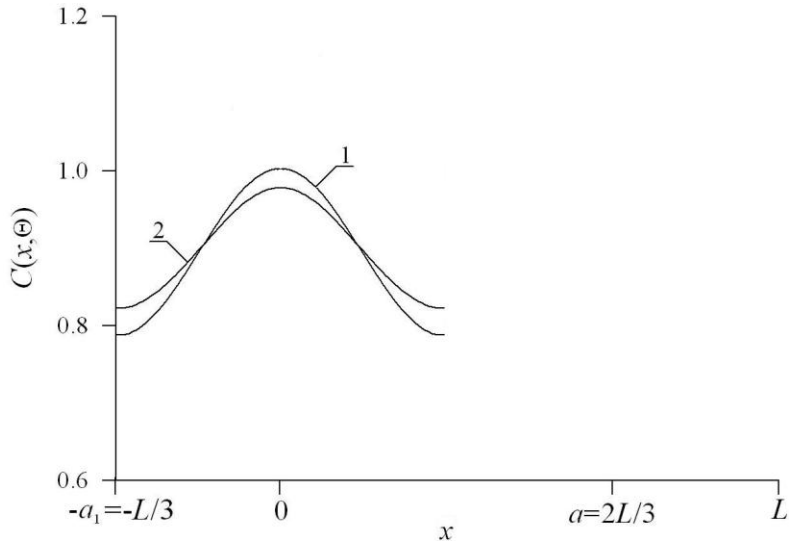


Fig. 4. Distributions of concentration of dopant.

Dopant concentration profiles in the central section of the epitaxial layer from *Fig. 1* along the direction parallel to the interface between the epitaxial layer and the substrate. The difference between dopant diffusion coefficients increases with the number of curves. In this section, the dopant diffusion coefficient is lower than in the adjacent regions.

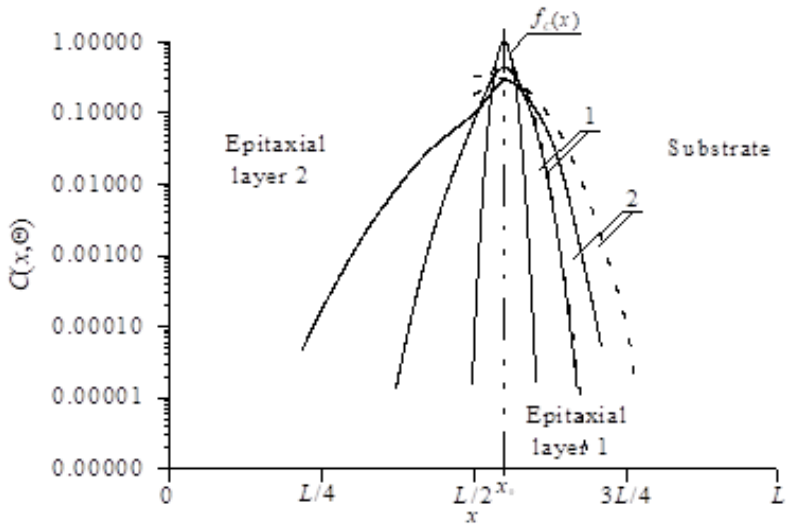


Fig. 5. Calculated distributions of implanted dopant in epitaxial layers of heterostructure.

Solid lines represent the spatial distributions of implanted dopants in a system consisting of two epitaxial layers, while dashed lines correspond to the distributions in a single epitaxial layer. The annealing time increases with the number of curves.

It should be noted that, within the framework of the proposed approach, the annealing process for dopants and/or radiation defects must be optimized. For this purpose, we employed a recently introduced optimization criterion [21–26]. The method is based on approximating the actual dopant distribution using a stepwise function $\psi(x,y,z)$, as illustrated in *Figs. 6* and *7*. The optimal annealing times are then determined by minimizing the mean-squared error between the target and actual distributions.

$$U = \frac{1}{L_x L_y L_z} \int_0^{L_x} \int_0^{L_y} \int_0^{L_z} \left[C(x,y,z,\Theta) - \psi(x,y,z) \right] dz\,dy\,dx \qquad (5)$$

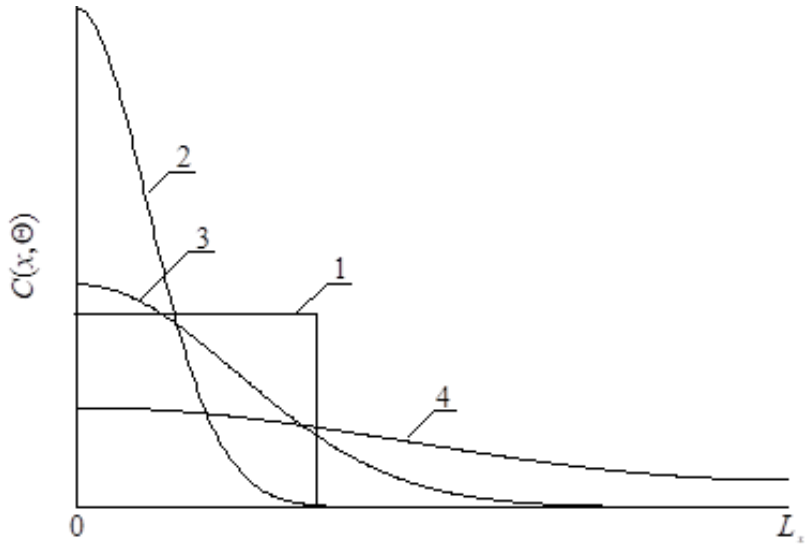


Fig. 6. Distributions of concentration of infused dopant in depth of heterostructure.

Figs. 6 and *7* Comparison of dopant concentration distributions for different annealing times. Curves 2–4 correspond to different annealing times, while Curve 1 represents the idealized stepwise approximation. An increase in the curve number corresponds to an increase in annealing time.

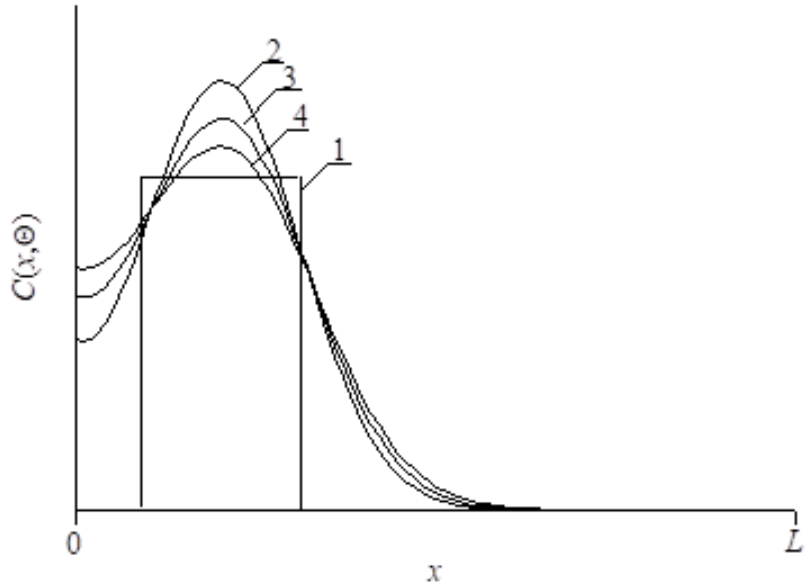


Fig. 7. Distributions of concentration of implanted dopant in depth of heterostructure.

Curves 2–4 in *Fig. 8* represent dopant concentration distributions for different annealing times, while Curve 1 corresponds to the idealized stepwise approximation. An increase in the curve number indicates a longer annealing time.

Figs. 8 and *9* shows the optimal annealing times as functions of the relevant process parameters. It is well known that a standard step in the fabrication of ion-doped structures is the annealing of radiation-induced defects. Ideally, upon completion of annealing, the dopant reaches the interface between the heterostructure layers. If the dopant does not have sufficient time to reach the interface, additional annealing may be required. *Fig. 9* illustrates the optimal values of this additional annealing time for the same set of parameters as in *Fig. 8*.

It is observed that the necessity to anneal radiation defects generally results in lower optimal annealing times for implanted dopants compared to the optimal annealing times required for diffused dopants. This behavior reflects the interplay between defect removal and dopant redistribution during the thermal treatment process.

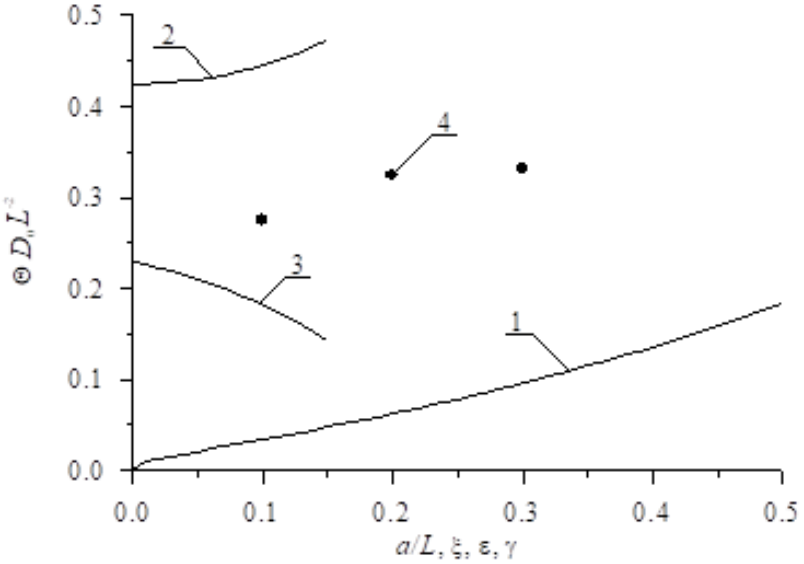


Fig. 8. Dimensionless optimal annealing time of infused dopant as a function of several parameters.

Fig. 9. Dependence of optimal annealing time on various parameters: Curve 1 represents the dependence on the ratio a/L with $\xi = \gamma = 0$ and equal dopant diffusion coefficients throughout the heterostructure. Curve 2 shows the dependence on the parameter ε for $a/L = 1/2$ and $\xi = \gamma = 0$ Curve 3 illustrates the dependence on the parameter ξ for $a/L = 1/2$ and $\varepsilon = \gamma = 0$ Curve 4 corresponds to the dependence on the parameter γ for $a/L = 1/2$ and $\varepsilon = \xi = 0$.

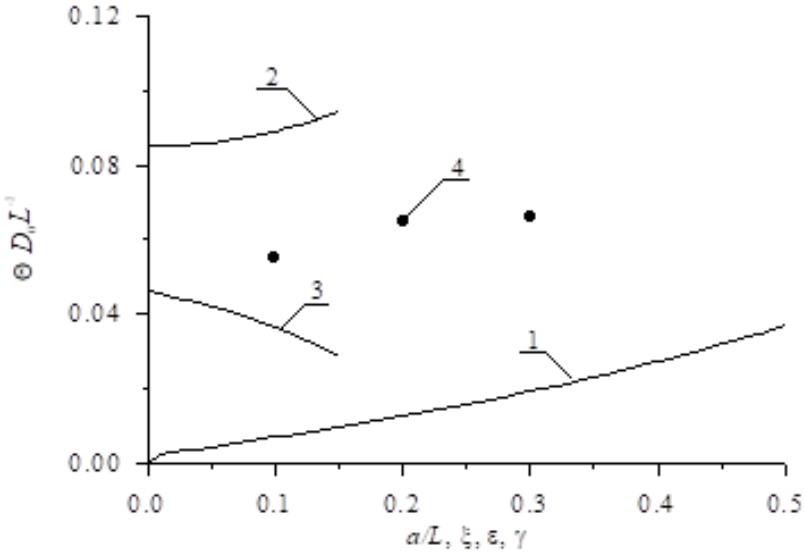


Fig. 9. Dimensionless optimal annealing time of implanted dopant as a function of several parameters.

Fig. 9. Dependence of optimal annealing time on various parameters: Curve 1 represents the dependence on the ratio a/L with $\xi = \gamma = 0$ and uniform dopant diffusion coefficients throughout the heterostructure. Curve 2 shows the dependence on the parameter ε for $a/L = 1/2$ and $\xi = \gamma = 0$. Curve 3 illustrates the dependence on the parameter ξ for $a/L = 1/2$ and $\varepsilon = \gamma = 0$. Curve 4 corresponds to the dependence on the parameter γ for $a/L = 1/2$ and $\varepsilon = \xi = 0$ [27].

4 | Conclusion

In this paper, we propose a novel approach to enhance the integration density of complementary gate overlap field-effect heterotransistors within the framework of a double-tail comparator. The proposed method allows for a significant reduction in the footprint of individual transistors while introducing only a minimal increase in their thickness. By optimizing the heterostructure design and doping profiles, this approach not only

improves the compactness of the circuit elements but also preserves their electrical performance. The resulting increase in integration density provides a pathway for developing more complex and highly functional comparator circuits without compromising device reliability or operational speed

References

[1] Bet, S., Quick, N., & Kar, A. (2007). Effect of laser field and thermal stress on diffusion in laser doping of SiC. *Acta materialia*, *55*(20), 6816–6824. https://doi.org/10.1016/j.actamat.2007.08.039

[2] Jung, J. W., Roh, J. S., Lee, Y., & Lee, K. (2000). Two-step rapid thermal annealing (TS-RTA) to suppress out-diffusion of dopants without degrading short channel effect of transistor. *IEEE electron device letters*, *21*(8), 376–377. https://doi.org/10.1109/55.852955

[3] Pankratov, E. L. (2004). Acceleration and deceleration of dopant diffusion in a semiconductor by space and time modulation of diffusion coefficient. *Journal of molecular liquids*, *114*(1–3), 179–185. https://doi.org/10.1016/j.molliq.2004.02.017

[4] Pankratov, E. L. (2008). Redistribution of dopant, implanted in a multilayer structure for production of ap--n-junction, during annealing radiative defects. *Physics letters a*, *372*(11), 1897–1903. https://doi.org/10.1016/j.physleta.2007.10.058

[5] Cubaynes, F. N., Stolk, P. A., Verhoeven, J., Roozeboom, F., & Woerlee, P. H. (2001). The influence of polysilicon gate morphology on dopant activation and deactivation kinetics in deep-submicron CMOS transistors. *Materials science in semiconductor processing*, *4*(4), 351–356. https://doi.org/10.1016/S1369-8001(00)00173-6

[6] Moore, G. E. (1965). Cramming more components onto integrated circuits. *McGraw-Hill New York*. https://doi.org/10.1109/N-SSC.2006.4785860

[7] Dennard, R. H., Gaensslen, F. H., Yu, H. N., Rideovt, V. L., Bassous, E., & Leblanc, A. R. (2007). Design of ion-implanted MOSFET's with very small physical dimensions. *IEEE solid-state circuits society newsletter*, *12*(1), 38–50. https://doi.org/10.1109/N-SSC.2007.4785543

[8] Sze, S. M., & Ng, K. K. (2007). Chapter 3 metal-semiconductors contacts. *Physics of semiconductor devices, 3rd ed.; john wiley & sons: Hoboken nj, usa*, 134–196. https://doi.org/10.1002/0470068329

[9] Cristiano, F., Shayesteh, M., Duffy, R., Huet, K., Mazzamuto, F., & Qiu, Y. (2016). Defect evolution and dopant activation in laser annealed Si and Ge. *Materials science in semiconductor processing*, *42*, 188–195. https://doi.org/10.1016/j.mssp.2015.09.011

[10] Alford, T. L., Thompson, D. C., Mayer, J. W., & Theodore, N. D. (2009). Dopant activation in ion implanted silicon by microwave annealing. *Journal of applied physics*, *106*(11). https://doi.org/10.1063/1.3260245

[11] Zhao, Z., David Theodore, N., Vemuri, R. N. P., Das, S., Lu, W., Lau, S. S., & Alford, T. L. (2013). Effective dopant activation via low temperature microwave annealing of ion implanted silicon. *Applied physics letters*, *103*(19). https://doi.org/10.1063/1.4829153

[12] Tabata, T., Rozé, F., Alba, P. A., Halty, S., Raynal, P.-E., Karmous, I., & Mazzamuto, F. (2021). Solid phase recrystallization and dopant activation in arsenic ion-implanted silicon-on-insulator by uv laser annealing. *2021 20th international workshop on junction technology (IWJT)* (pp. 1–5). IEEE. https://doi.org/10.48550/arXiv.2111.07577

[13] Alford, T. L., Gadre, M. J., Vemuri, R. N. P., & Theodore, N. D. (2012). Susceptor-assisted microwave annealing for activation of arsenic dopants in silicon. *Thin solid films*, *520*(13), 4314–4320. https://doi.org/10.1016/j.tsf.2012.02.086

[14] Plummer, J. D. (2009). *Silicon VLSI technology: Fundamentals, practice and modeling*. Pearson education India. https://www.researchgate.net/publication/230823028

[15] Razavi, B. (2005). *Design of analog CMOS integrated circuits*. Tsinghua university press Co., Ltd. https://www.amazon.com/Design-Analog-CMOS-Integrated-Circuits/dp/1259255093

[16] Mathur, V. K., Mak, P. S., & Lee, C. H. (1980). Carrier relaxation mechanisms in CdS0. 5Se0. 5 optoelectronic switches. *Journal of applied physics*, *51*(9), 4889–4893. https://doi.org/10.1063/1.328326

[17] Cowern, N. E. B., Janssen, K. T. F., de Walle, G. F. A., & Gravesteijn, D. J. (1990). Impurity diffusion via an intermediate species: The B-Si system. *Physical review letters*, *65*(19), 2434. https://doi.org/10.1103/PhysRevLett.65.2434%0A%0A

[18] Lindhard, J., Scharff, M., & Schiott, H. E. (1963). *Range concepts and heavy ion ranges* (Vol. 33). Munksgaard copenhagen. https://gymarkiv.sdu.dk/MFM/kdvs/mfm 30-39/mfm-33-14.pdf

[19] Özicsik, M. N. (1993). *Heat conduction*. John wiley & sons. https://www.amazon.com/Heat-Conduction-2nd-Necati-zisik/dp/0471532568

[20] Hinch, E. J. (1991). *Perturbation methods*. Cambridge university press. https://doi.org/10.1017/CBO9781139172189

[21] Fahey, P. M., Griffin, P. B., & Plummer, J. D. (1989). Point defects and dopant diffusion in silicon. *Reviews of modern physics*, *61*(2), 289. https://d1wqtxts1xzle7.cloudfront.net/121426719

[22] Kim, Y., Massoud, H. Z., & Fair, R. B. (1990). The effect of annealing ambient on dopant diffusion in silicon during low-temperature processing. *Journal of the electrochemical society*, *137*(8), 2599–2603. https://scholars.duke.edu/publication/687623

[23] Kim, Y., Massoud, H. Z., & Fair, R. B. (1989). The effect of ion-implantation damage on dopant diffusion in silicon during shallow-junction formation. *Journal of electronic materials*, *18*(2), 143–150. https://doi.org/10.1007/BF02657400%0A%0A

[24] Pichler, P., Ortiz, C. J., Colombeau, B., Cowern, N. E. B., Lampin, E., & Uppal, S. (2006). Diffusion and activation of dopants in silicon and advanced silicon-based materials. *Physica scripta*, *2006*(T126), 89–96. DOI 10.1088/0031-8949/2006/T126/021%0A%0A

[25] Pelaz, L., Marqués, L. A., Aboy, M., López, P., & Barbolla, J. (2005). Atomistic modeling of dopant implantation and annealing in Si: Damage evolution, dopant diffusion and activation. *Computational materials science*, *33*(1–3), 92–105. https://doi.org/10.1016/j.commatsci.2004.12.043

[26] Pankratov, E. L., & Bulaeva, E. A. (2014). Optimization of annealing of dopant to increase sharpness of p--n junctions in a heterostructure with drain of dopant. *Applied nanoscience*, *4*(5), 537–541. https://www.semanticscholar.org/paper/

[27] Pankratov, E. L. (2023). Amodel of manufacturing of a mosfet-filter with account mismatch-induced stress and porosity of materials on increasing of density of elements. *International journal of nanoscience, 7*(4), 187-197. https://www.academia.edu/download/110792954/9423antj01.pdf